Carrier confinement effects of $In_xGa_{1-x}N$/GaN multi quantum disks with GaN surface barriers grown in GaN nanorods

Youngsin Park[a], Christopher C. S. Chan[b,e], Robert A. Taylor[b,*], Nammee Kim[c], Yongcheol Jo[d], Seung W. Lee[d], Woochul Yang[d], and Hyunsik Im[d,**]

[a]*School of Natural Science, Ulsan National Institute of Science and technology (UNIST), Ulsan 44919, Korea*

[b]*Clarendon Laboratory, Department of Physics, University of Oxford, Oxford, OX1 3PU, UK*

[c]*Department of Physics, Soongsil University, Seoul 06978, Korea*

[d]*Division of Physics and Semiconductor Science, Dongguk University, Seoul 04620, Korea*

[e]*Department of Physics, Hong Kong University of Science and Technology, Clear Water Bay, Hong Kong, China*

Abstract: Structural and optical properties of $In_xGa_{1-x}N$/GaN multi quantum disks (QDisks) grown on GaN nanorods by molecular beam epitaxy have been investigated by transmission electron microscopy and micro-photoluminescence (PL) spectroscopy. Two types of InGaN QDisks were grown: a pseudo-3D confined InGaN pillar-type QDisks embedded in GaN nanorods; and QDisks in flanged cone type GaN nanorods. The PL emission peak and excitation dependent PL behaviour of the pillar-type Qdisks differ greatly from those of the flanged cone type QDisks. Time resolved PL was carried out to probe the differences in charge carrier dynamics. The results suggest that by constraining the formation of InGaN QDisks within the centre of the nanorod, carriers are restricted from migrating to the surface, decreasing the surface recombination at high carrier densities.

Keywords: InGaN/GaN quantum disk, Photoluminescence, Quantum confined Stark effect

[*]Corresponding author.
[**]Corresponding author.
E-mail: robert.taylor@phys.ox.ac.uk (R.A.Taylor), hyunsik7@dongguk.edu (H.Im).

1. Introduction

Nanowires or nanorods in III-nitride semiconductors are known to have great potential in fundamental physical science and novel technological applications due to the large bandgap and excellent structural confinement produced by heterostructures involving Ga, In and Al alloys [1,2]. The fabrication of optoelectronic devices with relatively low power consumption has already been demonstrated [3,4]. Reducing the dimensionality of a material enhances device performance, i.e., higher quantum efficiency, improved optical gain, and an increase of the exciton binding energy due to quantum confinement effects. $In_xGa_{1-x}N$/GaN heterostructures are particularly promising for applications such as light emitting diodes (LEDs) and laser diodes (LDs), as changing the indium mole fraction (x) in the active region can result in devices that operate at wavelengths from the visible to infrared (IR) [5]. However, it is well known that wurzite III-nitride structures with (0001) surface orientation have pyroelectric and built-in piezoelectric properties leading to strong electric fields along the crystal *c*-axis. This results in tilting of the electronic band structures at heterostructure interfaces giving rise to the quantum confined Stark effect (QCSE) [6-9], which is detrimental to the quantum efficiency of quantum confined nanostructures. The reduction in exciton oscillator strength is affected by both strong piezoelectric and spontaneous polarization fields. Non-polar substrates or one-dimensional nanowire structures have thus been used for growing the III-nitride nanostructures to mitigate such detrimental effects [10-15].

In this study, we report the optical characterization of InGaN/GaN multi quantum disks (QDisks) with different confined states grown on the tip of GaN nanorods. The structural characterization was investigated by a high-resolution field emission scanning electron microscopy (FESEM) and transmission electron microscopy (TEM). The optical transitions of the quantum confined state was characterized by micro-photoluminescence (μ-PL) and time resolved photoluminescence (TRPL).

2. Experimental

The samples used in this study were grown on Si (111) substrates by using rf-plasma assisted molecular beam epitaxy (PAMBE) without any buffer layers. By controlling the III/V ratio, the dimensions of the nanorods such as diameter, density, and height can be controlled. Detailed growth conditions have been reported in previously published literature [16-18]. After the successful formation of the GaN nanorods, 5 periods $In_xGa_{1-x}N$/GaN multi-QDisks were grown on the nanorod tips. The formation of the InGaN/GaN structures was confirmed by using a high-resolution FESEM and TEM. The In mole fraction of the InGaN disks was estimated by interpolation of a high resolution X-ray diffraction pattern measured from an InGaN epilayer grown under the same conditions. This value has been confirmed by measuring the lattice constant of the inter-plane spacing in a TEM image.

For macro-PL measurements, a He-Cd laser operating at 325 nm wavelength was used as an excitation light source with the power of 30 mW. A frequency-tripled femtosecond Ti:sapphire laser (100 fs pulses at 80MHz) operating at 266 nm was used for excitation of the QDisks for all of the μ-PL experiments. The sample was mounted in a continuous-flow helium cryostat, allowing the temperature to be controlled accurately from 4.2 K to room temperature. A 36× reflecting objective (Ealing) was mounted on a piezo controlled stage and held above the cryostat to both focus the incident laser beam to a spot size of ~0.8 μm^2 and to collect the sample luminescence. The luminescence was then directed to a spectrometer with a spectral resolution of ~700 μeV and a corresponding measured spatial resolution of 0.8 μm. The signal was finally detected using a cooled charge coupled device (CCD) detector. TRPL measurements were carried out using the same experimental set up as above, but in place of the CCD, the PL was directed towards a PMT connected to a commercial time correlated single photon counting system (Becker & Hickl SPC-134). Measurements of the lifetimes of the confined states were then carried out for a range of excitation power densities.

3. Results and discussion

Figures 1(a) and 1(b) show the FESEM images of the InGaN/GaN QDisks grown on a tip of GaN nanorods in cross-sectional and plan view, respectively. The total length of the nanorods varies from rod to rod, resulting in a QDisk size distribution and shape. Interestingly, the shape of the QDisks varies between rods, as can be seen at the tips and middles of GaN nanorods. In contrast to the QDisks grown on shorter host nanorods marked as red rectangles, the QDdisks grown on the longer rods exhibit a flanged cone like form marked with a blue rectangle in the figure. The circled area in Fig. 1(b) corresponds to the ~1.5 μm spot size of the laser beam used to probe the sample in the μ-PL measurements. The density of the nanorods is about ~10^9/cm^2 such that approximately 10 nanorods were excited at any one time. μ-PL measurements would hence reduce the ensemble effect from the large number of nanorods. The size distribution of QDisks made it possible to find spectrally isolated emission from single rods.

Figure 2 shows TEM images of QDisk regions with different shapes. Note that the shape of the QDisks depends on the length of GaN nanorods, with shorter rods typically showing a wire like structure. Figure 2(a) shows a multi-QDisk region at the tip of a relatively short nanorod. Both the nanorod and the InGaN/GaN multi-QDisk regions are clearly resolved. When indium atoms incorporate into the GaN region to form InGaN, the difference in lattice constant of the ternary alloy results in a slightly increased diameter compared to that of the host nanorod. The InGaN QDisks and GaN region can be clearly observed as dark and bright regions, respectively. A TEM image for InGaN/GaN multi-QDisks grown on a relatively long nanorod is presented in Fig. 2(b). In contrast to the image in Fig. 2(a), the image shows a flanged cone like structure, implying a lattice constant variation. The side wall of the InGaN/GaN region is rough, and moreover, there is very little contrast with which to distinguish between the GaN and InGaN layers.

Zoomed high resolution TEM images of the InGaN/GaN regions of Figs. 2(a) and (b) are

presented in Figs. 2(c) and (d), respectively, with an intensity profile as a function of distance. Figure 2(c) shows a high magnification TEM image of the marked region in Fig. 2(a). The InGaN layers are surrounded by both vertical and lateral (side wall) GaN layers, providing confinement in the vertical and lateral direction. For the pillar type multi-QDisks, the lattice constant is constant and measured to be 0.263 nm corresponding to the (0002) plane for the $In_xGa_{1-x}N$ from the fringe analysis. This lattice constant corresponds to an indium content x of ~ 0.1. In the case of flanged cone type multi-QDisks, the InGaN layers are not confined laterally by any GaN barrier. The lattice constant varies from atomic layer to layer, which implies a composition fluctuation in the $In_xGa_{1-x}N$/GaN region.

Figure 3 shows the macro- and micro-PL spectra of the InGaN/GaN multi-QDisks taken at a temperature of 10 K. In the case of macro-PL measurements, we observe a broad emission below 3.4 eV originating from the ensemble of InGaN QDisks. The exciton transition of the GaN nanorods (I_2 or D^0X) and the recombination of excitons bound to the (so-called I_1) basal stacking faults (BSFs) is also clearly observed. In the case of μ-PL experiments, however, several sharp emission peaks corresponding to individual nanorods can be observed. First, the laser spot was focused on the tip of nanorods in Fig. 1(a) (long nanorods). A strong and sharp luminescence near 3.263 eV (red spectrum - labeled as P1) with a full width at half maximum (FWHM) of ~5.4 meV was observed originating from the flanged cone type InGaN/GaN multi-QDisks. By controlling the piezoelectric stage of the PL objective, the laser spot focal plane was lowered to focus onto the tips of shorter nanorods. The P1 peak almost disappears and new peaks (blue spectrum) near 3.354 eV and 3.365 eV, which are labeled as P2 and P3, respectively, are observed. These are identified as originating from InGaN/GaN regions with a pillar type structure.

Figures 4(b) and 4(c) show the excitation power-dependent μ-PL spectra of the P1, P2, and P3 peaks measured at 4.2 K. The PL energy of P1 peak is observed to be blueshifted by ~2

meV as the excitation intensity is increased to ~4 kW/cm^2 due to both piezo-electric field screening of the QDisk, and also filling of localized states, before saturating with any further increase in excitation power [9, 19]. A similar small shift of about 2 meV has been previously reported in GaN quantum dots that were subjected to a lateral electric field [20]. The PL energy of the P2 and P3 peaks, however, does not change with increasing excitation power. The results indicate that the field screening induced blueshift due to the QCSE is either reduced in the pillar type InGaN QDisk laterally surrounded by GaN, or that the dominant mechanism which blueshifts the InGaN QDisk emission is altered by the side wall GaN barrier. In the similar structures of AlGaN/GaN with a 3-dimensionally confined QDisks, a reduction to the QCSE has previously been found [21].

The integrated PL intensity of the of the P1 and P2 peaks was presented in Fig 4(c). The PL intensity shows PL quenching starting to occur in Peak 1 at 4.53 kW/cm^2, which may originate from the non-radiative process onset from the carriers recombining on the surface. On the other hand, that of P2 peak retains the same rate of increase of PL intensity.

In order to further investigate the effect, we carried out TRPL measurements for the peaks P1 of 3.262 eV at low excitation power and 3.265 eV at high excitation power and P2 (3.354 eV). Figures 5(a) and 5(b) show the TRPL spectra measured at 4.2 K with different excitation intensities of ~0.58 kW/cm^2 and ~8.5 kW/cm^2, respectively. The decay curves were fitted by a bi-exponential decay of the form $I(t) = A_1 \exp(-t/\tau_1) + A_2 \exp(-t/\tau_2)$. Here, the τ_1 and τ_2 are fast and slow decay time components, respectively. At the low excitation intensity of ~0.58 kW/cm^2, the decay time is deduced to be about 0.58±0.03 ns for the fast component and about 5.75±0.48 ns for the slow component for both P1 and P2 peaks, which shows an almost similar trace. Though the TRPL decay curve of non-polar InGaN/GaN quantum wells usually shows an exponential trace due to excitonic recombination [22,23], there are reports showing that non-exponential decay can arise due to carrier localization which has been modelled with by

pseudo-donor-acceptor pair recombination [23-27]. The non-exponential behavior is due to tightly localized carriers resulting from the combined effect of the piezoelectric field and also indium alloy fluctuations in the InGaN epilayer. The separation of the recombining carrier pairs dominates the radiative recombination lifetime [23]. The distribution of different separation lengths is responsible for the non-exponential decay trace. At the high excitation intensity of ~8.5 kW/cm^2, however, the decay trace shows quite different characteristics. For the P1 peak, a fast component of ~0.54±0.013 ns time constant dominates the lifetime measurement. The P2 peak, however, shows no such decrease in recombination lifetime. The normalized decay curves of peak P2 (3.354 eV) for the two excitation power densities are shown in inset in Fig. 5(b). Surprisingly, the dynamics of the emission of peak P2 are unaffected by the 15-fold increase in power density (reaching peak powers densities in excess of 1GW/cm^2).

Non-radiative recombination pathways can decrease the measured PL lifetime and quench PL intensity [25,28]. In the side wall confined disks, decrease in lifetime is not observed for the same excitation power. This leads us to speculate that for the QDisks without sidewall barriers, a proportion of the carriers may be recombining at the surface. As carrier density increases in the well layer, the localized states are first populated randomly, and the band is gradually filled with more energetic carriers. These energetic carriers can in principle, migrate to the surface, if the energy barrier caused by the air-InGaN surface potential bending at the sidewalls of the QDisks is relatively low [29], provided that the carrier mobility in InGaN is high enough at the experimental temperatures. The observations do indeed support the inference that the carrier density has less effect on the recombination dynamics in the pillar type structure with GaN surface barriers as opposed to the flange type.

Although the TRPL results in Fig. 5(b) indicate a reduction in the lifetime for the flange type QDisk and not for the pillar-confined type, it is not entirely true that the QCSE is mitigated in the pillar type QDisks. The lifetime of P2 is consistently longer than that of P1, despite the

higher energy emission. A higher emission photon energy due to tighter quantum confinement and lower indium content should both decrease the recombination lifetime, contrary to what we observe. We suspect that surface effects play a significant role in the recombination dynamics seen in our nanorods. It has been reported that carriers can have lateral separation on the plane of the InGaN quantum disk due to the valence and conduction band bending at the side walls of the nanorods from the surface Fermi level [25]. The lateral confinement of the quantum well in the pillar structure can prevent carriers from diffusing to the surface of the nanorod, and thus reducing the non-radiative surface recombination probability.

4. Conclusion

We have investigated the structural and optical properties of the $In_xGa_{1-x}N$/GaN multi quantum disks grown on GaN nanorods by molecular beam epitaxy. Two types of InGaN quantum disks were grown at the same time, that is to say, one is the InGaN quantum disk embedded in a pillar GaN nanorod and the other is a multi-stacked structure with flanged cone type GaN nanorods. A strong emission near 2.6 eV with a FWHM of ~5.4 meV has been observed originating from the flanged like cone type quantum disk. While the emission peak relating to the quantum dot like quantum disks was observed not to be shifted, those relating to flanged like cone type disks blueshifted with increasing excitation power due to mainly band tail state filling. The time-resolved photoluminescence of the emission lines as a function of excitation powers has also been investigated, and we conclude that the GaN barriers around the sidewalls of QDisks effectively reduce surfaces effects which are detrimental for recombination efficiency.

Acknowledgments

This research was supported by Basic Science Research Program (2015R1D1A1A01058332, 2016R1D1A1B03935688, 2015M2A2A6A02045251, and 2016R1A6A1A03012877), through the National Research Foundation of Korea (NRF).

References

1. F. A. Ponce, D. P. Bour, Nitride-based semiconductors for blue and green light-emitting devices, Nature 386 (1997) 351-359.
2. H. Morkoc, S. N. Mohammand, High-luminosity blue and blue-green gallium nitride light-emitting diodes, Science 267 (5194) (1995) 51-55.
3. C. M. Lieber, One-dimensional nanostructures: Chemistry, physics & applications, Solid State Commun. 107 (11) (1998) 607-616.
4. S. Nakamura, T. Mukai, M. Senoh, Candela -class high- b double -hetero structure blue light- emitting diodes , Appl. Phys. Lett. 64 (13) (1994) 1687-1689.
5. W. Shan, W. Walukiewicz, E. E. Haller, B. D. Litter, J. J. Song, M. D. McCluskey, N. M. Johnson, Z. C. Feng, M. Schurman, R. A. Stall, Optical properties of $In_xGa_{1-x}N$ alloys grown by metalorganic chemical vapor deposition, J. Appl. Phys. 84 (8) (1998) 4452-4458.
6. A. Bykhovski, B. Gelmont, M. Shur, The influence of the strain-induced electric field on the charge distribution in GaN-AlN-GaN structure, J. Appl. Phys. 74 (11) (1993) 6734-6739.
7. F. Bernardini, V. Fiorentini, D. Vanderbilt, Spontaneous polarization and piezoelectric constants of III-V nitrides, Phys. Rev. B 56 (1997) R10024.
8. M. J. Holmes, Y. S. Park, J. H. Warner, R. A. Taylor, Quantum confined Stark effect and corresponding lifetime reduction in a single InGaN quantum disk, Appl. Phys. Lett. 95 (18) (2009) 181910.
9. Y. S. Park, M. J. Holmes, T. W. Kang, R. A. Taylor, Quantum confined Stark effect of InGaN/GaN multi quantum disks grown on top of GaN nanorods, Nanotechnology 21 (11) (2010) 115401.
10. T. Wang, T. J. Puchtler, T. Zhu, J. C. Jarman, C. C. Kocher, R. A. Oliver, R. A. Taylor,

Temperature-dependent fine structure splitting in InGaN quantum dots, Appl. Phys. Lett. 111 (5) (2017) 053101.

11. T. Wang, T. J. Puchtler T. Zhu, J. C. Jarman, L. P. Nuttall, R. A. Oliver, R. A. Taylor, Polarization-controlled single photon emission at high temperatures from InGaN quantum dots, Nanoscale 9 (2017) 9421-9427.
12. M. Arita, F. L. Roux, M. J. Holmes, S. Kako, Y. Arakawa, Ultraclean single photon emission from a GaN quantum dot, Nano Lett. 17 (5) (2017) 2902-2907.
13. Z. Gacevic, M. Holmes, E. Chernysheva, M. Muller, A. Torres-Pardo, P. Veit, F. Bertram, J. Christen, J. M. G. Calbet, Y. Arakawa, E. Calleja, S. Lazic, Emission of linearly polarized single photons from quantum dots contained in nonpolar, semipolar, and polar sections of pencil-like InGaN/GaN nanowires, ACS Photo. 4 (3) (2017) 657-664.
14. M. J. Holmes, S. Kako, K. Choi, M. Arita, Y. Arakawa, Spectral diffusion and its influence on the emission linewidths of site-controlled GaN nanowire quantum dots, Phys. Rev. B 92 (11) (2015) 115447.
15. M. J. Holmes, S. Kako, K. Choi, P. Podemski, M. Arita, Y. Arakawa, Probing the excitonic states of site-controlled GaN nanowire quantum dots, Nano Lett. 15 (2) (2015) 1047-1051.
16. Y. S. Park, S. H. Lee, J. E. Oh, C. M. Park, T. W. Kang, Self-assembled GaN nanorods grown directly on (111) Si substrates: Dependence on growth conditions, J. Crystal Growth 282 (3-4) (2005) 313-319.
17. Y. S. Park, C. M. Park, D. J. Fu, T. W. Kang, J. E. Oh, Photoluminescence studies of GaN nanorods on Si (111) substrates grown by molecular-beam epitaxy, Appl. Phys. Lett. 85 (23) (2004) 5718-5720.
18. C. M. Park, Y. S. Park, H. Im, T. W. Kang, Optical properties of GaN nanorods grown by molecular-beam epitaxy; dependence on growth time, Nanotechnology 17 (2006) 952-955.
19. N. Shimosako, Y. Inose, H. Satoh, K. Kinjo, T. Nakaoka, T. Oto, K. Kishino, and K. Ema

"Carrier-density dependence of photoluminescence from localized states in InGaN/GaN quantum wells in nanocolumns and a thin film", J. Appl. Phys.118, 175702 (2015).

20. T. Nakaoka, S. Kako, Y. Arakawa, Unconventional quantum-confined Stark effect in a single GaN quantum dot, Phys. Rev. B 73 (12) (2006) 121305.
21. Y. S. Park, C. C. S. Chan, B. P. L. Reid, M. J. Holmes, D. M. Coles, J. A. Alexander-Webber, R. J. Nicholas, R. A. Taylor, S.-W. Lee, W. Yang, H. Im, Reduced Stark shift in three-dimensionally confined GaN/AlGaN asymmetric multiquantum disks, Opt. Mat. Exp. 5 (4) (2015) 849-857.
22. S. Marcinkevicius, K. M. Kelchner, L. Y. Kuritzky, S. Nakamura, S. P. DenBaars, J. S. Speck, Photoexcited carrier recombination in wide *m*-plane InGaN/GaN quantum wells, Appl. Phys. Lett. 103 (11) (2013) 111107.
23. P. Dawson, S. Schulz, R. A. Oliver, M. J. Kappers, C. J. Humphreys, The nature of carrier localization in polar and nonpolar InGaN/GaN quantum wells, J. Appl. Phys. 119 (18) (2016) 181505.
24. A. Morel, P. Lefebvre, S. Kalliakos, T. Taliercio, T. Bretagnon, B. Gil, Donor-acceptor-like behavior of electron-hole pair recombinations in low-dimensional (Ga, In)N/GaN systems, Phys. Rev. B 68 (4) (2003) 45331.
25. Y. J. Wang, S. J. Xu, D. G. Zhao, J. J. Zhu, H. Yang, X. D. Shan, D. P. Yu, Non-exponential photoluminescence decay dynamics of localized carriers in disordered InGaN/GaN quantum wells: the role of localization length, Opt. Exp. 14 (26) (2006) 13151-13157.
26. S.-W. Feng, Y.-C. Cheng, C.-C. Liao, Y.-Y. Vhung, C.-W. Liu, C.-C. Yang, Y.-S. Lin, K.-J. Ma, J.-I. Chyi, Two-component photoluminescence decay in InGaN/GaN multiple quantum well structures, Phys. Stat. Sol. (b) 228 (1) (2001) 121-124.
27. V. Liuolia, S. Marcinkevičius, Y.-D. Lin, H. Ohta, S. P. DenBaars, S. Nakamura, Dynamics of polarized photoluminescence in m-plane InGaN/GaN quantum wells, J. Appl. Phys. 108

(2010) 023101.

28. T. J. Badcock, M. Ali, T. Zhu, M. Pristovsek, R. A. Oliver, A. J. Shields, Radiative recombination mechanisms in polar and non-polar InGaN/GaN quantum well LED structures, Appl. Phys. Lett. 109 (15) (2016) 151110.
29. C. S. Chan, B. P. L. Reid, R. A. Taylor, Y Zhuang, P. A. Shields, D. W. E. Allsopp, W. Jia, Optical studies of the surface effects from the luminescence of single GaN/InGaN nanorod light emitting diodes fabricated on a wafer scale, Appl. Phys. Lett. 102 (11) (2013) 111906.

Figure captions

Figure 1. (a) Cross sectional scanning electron microscope image of the InGaN/GaN multi quantum disks grown on GaN nanorods. The rectangular regions contain InGaN/GaN multi quantum disks. The scale bar is 2 μm. (b) Plan view of scanning electron microscope for the InGaN/GaN multi quantum disks. The circle corresponds to the laser beam area.

Figure 2. (a) and (b) Transmission electron microscope image of the InGaN/GaN multi quantum disks as red and blue marked regions, respectively, in Fig. 1(a). (c) and (d), Transmission electron microscope image as shown in white rectangular regions in (a) and (b), respectively.

Figure 3. Photoluminescence spectra of the InGaN/GaN multi quantum disks measured at 10 K with different scan methods. The black spectrum is macro-photoluminescence excited by a He-Cd laser (325 nm). The red and blue spectra are micro-photoluminescence excited by a frequency-tripled Ti:sapphire laser (266 nm) with a beam diameter of ~1.5 μm. The red and blue spectra come from the upper and the lower squared regions of figure 1(a), respectively.

Figure 4. (a and b) Excitation-power dependent micro PL spectra of the P1 and P2 peaks, respectively. (c) Integrated PL intensity of the P1 and P2 peaks as a function of temperature.

Figure 5. Time resolved photoluminescence (TRPL) from the P1 and P2 peaks with two different excitation intensities of 0.58 kW/cm^2 for the 3.262 eV (a) and 8.5 kW/cm^2 for the 3.265 eV (b). The blue solid lines in (b) is the fitted line using bi-exponential decay curve. The inset in (b) depicts the TRPL of the P2 peak (3.354 eV) with excitation intensities of 0.58 kW/cm^2 and 8.5 kW/cm^2.

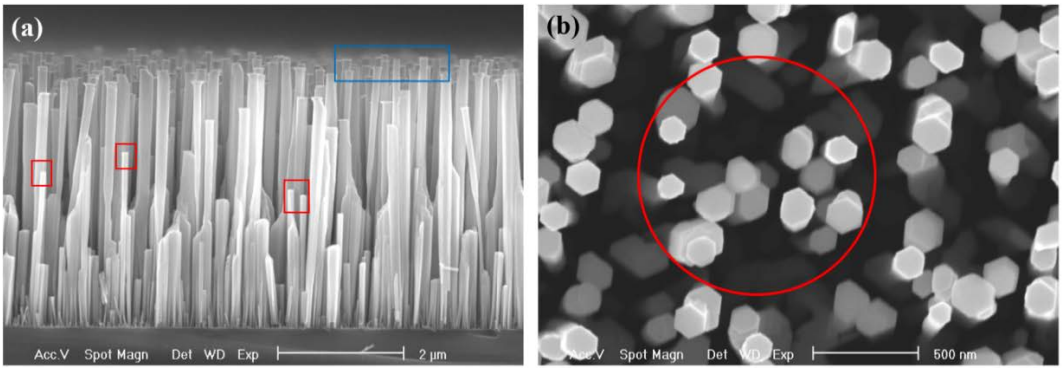

Park et al, Fig. 1

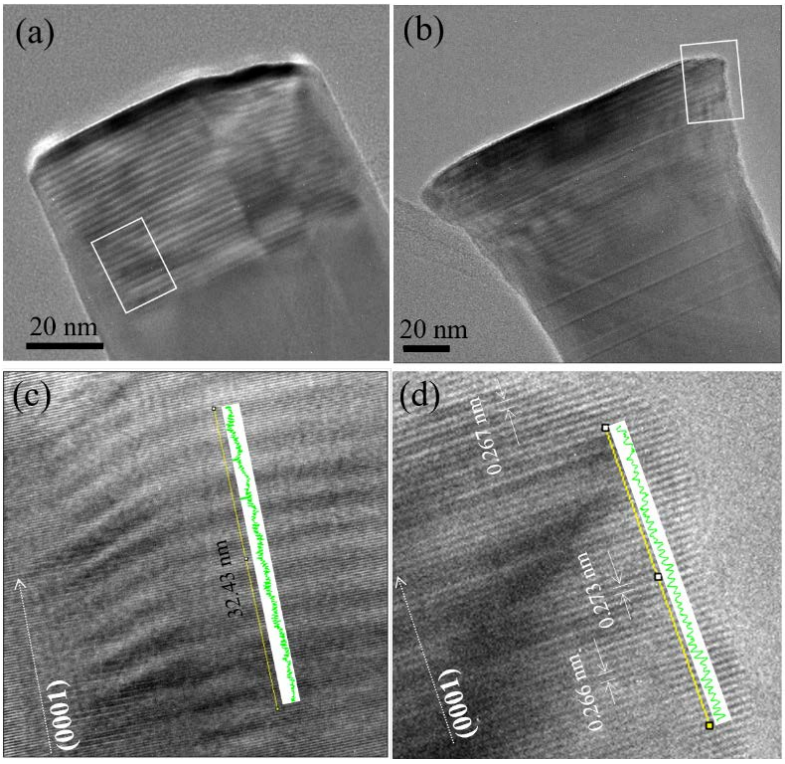

Park et al. Fig. 2.

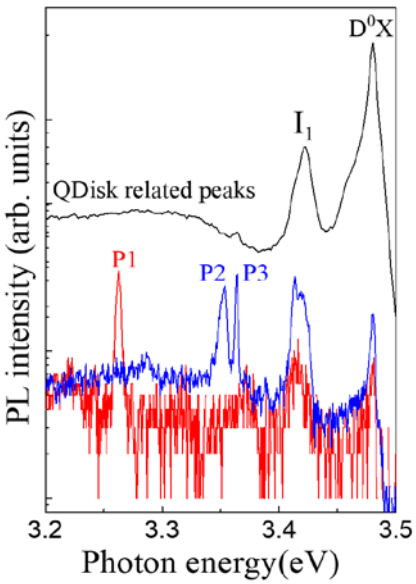

Park et al. Fig. 3.

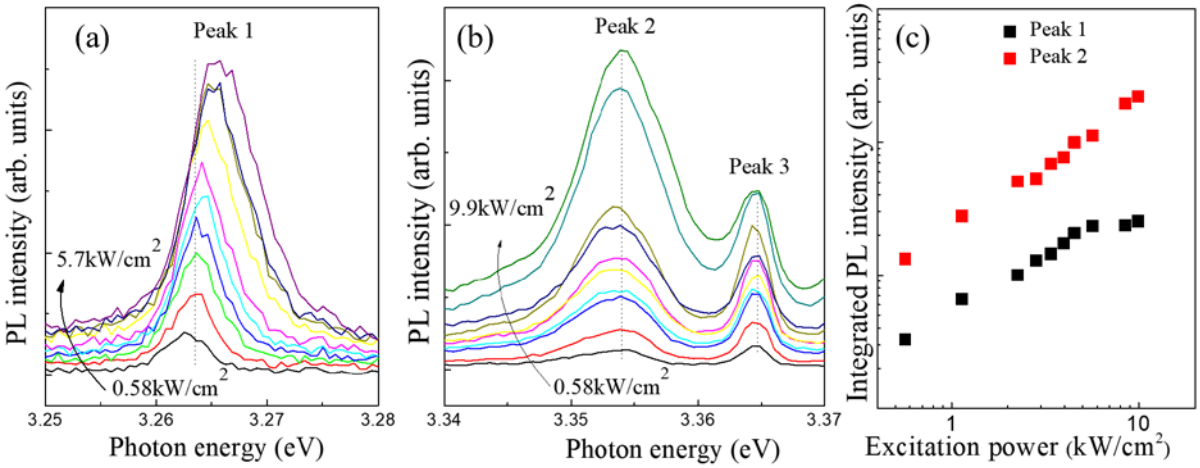

Park et al. Fig. 4.

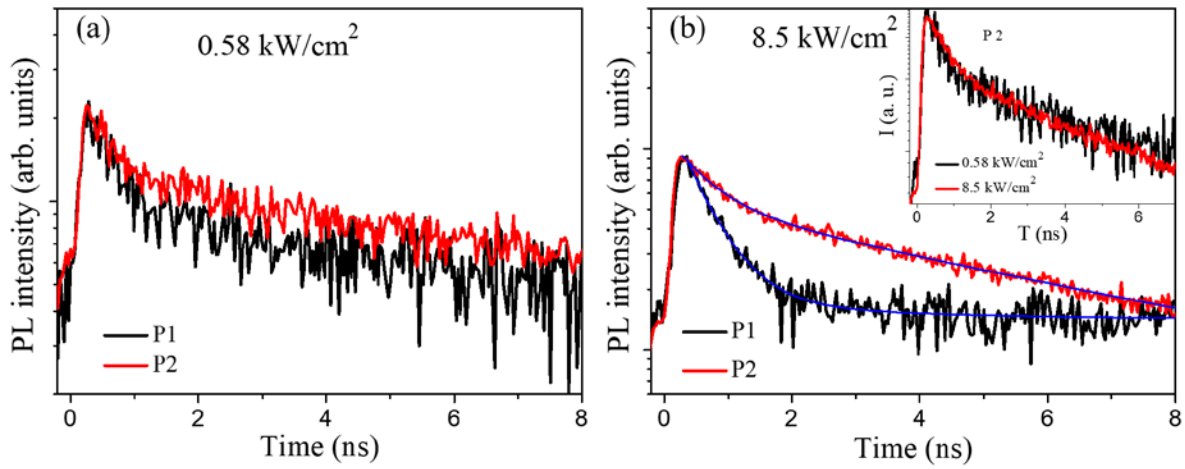

Park et al. Fig. 5